Taylor & Francis
Taylor & Francis Group

Check for updates

Structure assignment, conformational properties and discovery of potential targets of the Ugi cinnamic adduct NGI25

Nikitas Georgiou[a], Niki Gouleni[a], Eleni Chontzopoulou[a], George S. Skoufas[a], Anastasios Gkionis[a], Demeter Tzeli[b,c], Stamatia Vassiliou[a] and Thomas Mavromoustakos[a] (ID)

[a]Department of Chemistry, Laboratory of Organic Chemistry, National and Kapodistrian University of Athens, Athens, Greece; [b]Department of Chemistry, Laboratory of Physical Chemistry, National and Kapodistrian University of Athens, Athens, Greece; [c]Theoretical and Physical Chemistry Institute, National Hellenic Research Foundation, Athens, Greece

Communicated by Ramaswamy H. Sarma

ABSTRACT

The structure assignment and conformational analysis of cinnamic derivative N-benzyl-N-(2-(cyclohexylamino)-2-oxoethyl) cinnamamide (NGI25) was carried out through Nuclear Magnetic Resonance (NMR) spectroscopy, Molecular Dynamics (MD) and Quantum Mechanics (QM), i.e. semiempirical and Density Functional Theory (DFT) calculations. Moreover, Homonuclear (COSY, NOESY) and heteronuclear (HSQC, HMBC) experiments were applied to assign its protons and carbons. After structure identification, NGI25 was subjected to computational calculations to reveal its most favorable conformations. In particular, MD studies were performed in two different solvents, DMSO of intermediate polarity and hydrophobic $CHCl_3$. The obtained results suggest that NGI25 adopts similar conformations in both environments. In particular, the two aromatic rings of the molecule reside in spatial vicinity, while they remain quite distant from the cyclohexane. 2D NOESY experiments confirmed the *in silico* MD and QM calculations. Finally, molecular docking calculations were performed in order to reveal possible enzyme-targets for NGI25. Swiss target module was used to guide the discovery of new targets based on the structure of NGI. Indeed, it was predicted that NGI25 inhibited butyrylcholinesterase (BCHE) and lipoxygenase (LOX). Molecular docking experiments, followed by Molecular Dynamics studies, confirmed the favorable binding of NGI25 to both enzymes.

Abbreviations: AcOEt: Ethyl Acetate; Ax: axial; CDCl₃: chloroform; DMSO: dimethyl sulfoxide; Eq: equatorial; GLH: Glutamic acid; IMCRs: Isocyanide-based multicomponent reactions; MCRs: Multicomponent reactions; MD: Molecular dynamics; NMR: Nuclear magnetic resonance; PDB: Protein Data Bank; PE: Petroleum ether; PHE: Phenylalanine; THR: Threonine; TRP: Tryptophan

1. Introduction

Multicomponent reactions (MCRs), are widely defined as reactions in which three or more components are added to a single vessel at the same time to lead to a final product that contains most of the atoms from the starting reagents (Jieping Zhu, 2005). In as much as they meet many of the criteria dictated by green chemistry, this sustainable strategy has found many applications ranging from the production of fine chemicals to various uses in material sciences (Cioc et al., 2014; Dömling et al., 2012; Hulme & Gore, 2003; Ruijter & Orru, 2013; Theato, 2015; Touré & Hall, 2009).

Isocyanide-based multicomponent reactions (IMCRs) are effective and straightforward methods to access highly valuable molecules (Akritopoulou-Zanze, 2008; Luo et al., 2021). Since Passerini and Ugi demonstrated that the ambivalent reactivity of isocyanides could be successfully harnessed in multicomponent processes, this methodology never stopped

giving access to highly valuable molecules which have been widely used in drug discovery (Akritopoulou-Zanze, 2008), natural product synthesis (Graebin et al., 2019), biology (Basso et al., 2010), and materials science (Dömling, 2006).

As one of the most prominent IMCRs, the classic Ugi-4CR (Gruppen et al., 1959) using isocyanides, aldehydes, amines, and carboxylic acids (Scheme 1) is a powerful tool for the synthesis of peptoids. This reaction serves as an ideal tool for accessing large and diverse chemical space by creating up to five points of structural diversity in one-pot, which can be very useful for the expeditious syntheses of bioactive molecules (Fouad et al., 2020).

In this article the traditional Ugi-4CR reaction was utilized to synthesize the molecule under study N-benzyl-N-(2-(cyclohexylamino)-2-oxoethyl) cinnamamide, or its abbreviated name NGI25 (Figure 1).

A detailed conformational analysis of NG125 was carried out with multiple methods to obtain its most energetically

CONTACT Stamatia Vassiliou ✉ svassiliou@chem.uoa.gr ▣ Department of Chemistry, Laboratory of Organic Chemistry, National and Kapodistrian University of Athens, Panepistimioupolis Zografou, Athens, 11571, Greece; Thomas Mavromoustakos ✉ tmavrom@chem.uoa.gr ▣ Department of Chemistry, Laboratory of Organic Chemistry, National and Kapodistrian University of Athens, Panepistimioupolis Zografou, Athens, 11571, Greece.

Traditional Ugi-4CR

R_1NC + R_2CHO + R_3COOH + R_4NH_2 $\xrightarrow[\text{rt, 5 days}]{\text{MeOH}}$
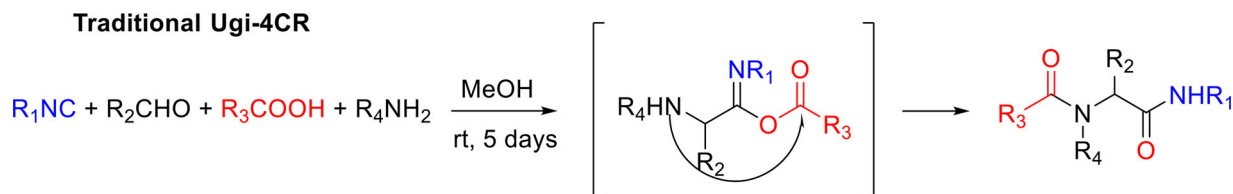
Scheme 1. Traditional Ugi-4CR reaction. For the synthesis of NGI25 $R_1=$ cyclohexyl, $R_2=$ H, $R_3=$ cinnamic der., $R_4=$ Bn
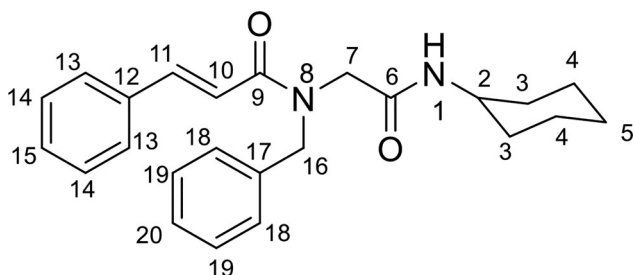
Figure 1. Structure of NGI25 with carbons numbered as these are used in the assignment of NMR spectra.

favored conformation. Specifically, NMR, molecular mechanics (*via* grid scan analysis), MD, semi-empirical PM6 method, and DFT methodology in chloroform ($CHCl_3$) and dimethylsoulf-oxide (DMSO) solvents have been applied. A wide range of conformations has been examined through PM6 and DFT calculations. Finally, molecular dynamics calculations were used to study the mobility of NGI25 in the two solvents DMSO and $CHCl_3$. Since the cinnamic acid derivative, NGI25, is a novel structure, it is sought for possible pharmacological targets through Swiss Target module. In order to justify the binding of NGI25 to predicted potential pharmacological targets, we performed molecular docking calculations to the predicted enzyme-targets. Two major targets were detected using Swiss Target module and literature data.

Thus, NGI25 was examined through Molecular Docking studies for its possible lipoxygenase (LOX) inhibition and its anti-butyrylcholinesterase (anti-BCHE) action for the treatment of Alzheimer disease. Molecular Docking results indicate that NGI25 binds strongly to both enzymes' active sites, while the value of ΔG_{bind} of NGI25 is more favorable compared to the ΔG_{bind} value of known LOX and BCHE inhibitors. *In silico* examination of the molecule's physical and chemical properties indicates that it is does not exert any toxic action, as predicted by SwissADME module (Daina et al., 2017).

2. Materials and methods

2.1. Synthesis of NGI25

$CDCl_3$, DMSO-d_6 and ultra-precision NMR tubes Wilmard 535–5 mm (SPINTEC ROTOTEC) were used for the NMR experiments. NGI25 was synthesized in our laboratory as it will be described below.

A solution of benzylamine (0.11 mL, 1.00 mmol), paraformaldehyde (0.03 g, 1.00 mmol) in MeOH (6 mL) was stirred for 5 h at room temperature. Cinnamic acid (0.15 g, 1.00 mmol), and cyclohexyl isocyanide (0.12 mL, 1.00 mmol)

were then added. The reaction mixture was stirred at room temperature for 5 d. The volatiles were removed and the crude product was purified with column chromatography using ethyl acetate and petroleum ether as eluents to give the desired product as white solid in 86% yield. $R_f=$ 0.54 [AcOEt/PE (40–60 °C) 2:3].

2.2. Conformational analysis

2.2.1. NMR spectroscopy

NMR spectra in DMSO-d6 solvent were obtained using 400 MHz Bruker Avance Spectrometer at 25 °C. All data were collected using pulse sequences and phase-cycling routines provided in the Bruker libraries of pulse programs (^{1}H: zg30, ^{13}C: zgpg30, 2D-COSY: cosygpmfqf, 2D-NOESY: noesygpphpp, 2D-HSQC: hsqcedetgpsisp (Cioc et al., 2014; Dömling et al., 2012). 2D-HMBC: hmbclpndqf). Data processing including sinebell apodization, fourier transformation, phasing symmetrization and plotting were performed using Bruker and MestreNova software package.

2.2.2. Grid scan

The software used for grid scan was Macromodel, which is available in Schrödinger Suites. The energy minimization and Grid Scan method was performed using OPLS2005 force field.

2.2.3. Molecular dynamics

The system for the MD (Imtiaz, Muzaffar, et al., 2021) studies was setup with DMSO or chloroform molecules surrounding the cinnamic compound. OPLS2005 force field was applied and the long-range electrostatics were treated with the particle mesh Ewald method (PME) (Essmann et al., 1995; Martyna et al., 1994) and a grid spacing of 0.8 Å. Van der Waals and short-range electrostatic interactions were smoothly truncated at 9.0 Å. Temperature was kept constant using the Nosé-Hoover thermostat (Humphreys et al., 1994) while the Martyna-Tobias-Klein method (Martyna et al., 1994) was used to control the pressure. Periodic boundary conditions were applied and the dimensions of the simulation box were (10.0 × 10.0 × 10.0) Å. The equations of motion were integrated using the multistep RESPA integrator (Lyman & Zuckerman, 2006) with an inner time step of 2 fs for bonded interactions and non-bonded interactions within a cut-off of 9 Å. An outer time step of 6.0 fs was used for non-bonded interactions beyond the cut-off. Each system was equilibrated using the default protocol provided in Desmond (D. E. Shaw Research, XXXX) Desmond relaxation protocol includes

minimization of the system firstly with the solute restrained and then with no restraints applied. The system was relaxed in the NVT ensemble using Berendesen thermostat with a fast temperature relaxation constant at $T = 10\,K$ for 1.0 ns, while the velocity resampling was set to 1 ps. Berendesen thermostat and Berendesen barostat have been used for the system's relaxation in the NPT ensemble using a temperature of 10 K with fast and slow pressure relaxation constant, while the system's pressure was set to 1 atm for 12 ps. The same thermostat and barostat have been used for the following simulation of 24 ps, where the system left to relax in $T = 298\,K$ and $P = 1 atm$. Before commencing with the production phase, the system was left to relax in the NPT ensemble with no restraints for 1.0 ns. The production phase of the MD simulation was set to 500 ns. The MD simulations were run in workstations using the GPU implementation of the MD simulations codes. The equilibration time was discarded and only the production phase was sampled to ensure adequate sampling.

The same parameters for MD studies have been applied for the simulations of 'enzyme-ligand' complexes. In these simulations, the complexes have been solvated with TIP3P water models, while the pressure was set to 1 atm and the temperature to 310 K, in order to study the stability of the ligands into the enzymes' cavities. The production phase of these simulations was set to 200 ns, which is an adequate computational time to observe a 'protein-ligand' complex.

2.2.4. Semi-empirical and DFT calculations

Finally, in addition to conformational analysis *via* molecular mechanics, conformational analysis was also carried out via the semi-empirical PM6 and the DFT(B3LYP (Lee et al., 1988; Becke, 1993)/6-311 + G(d,p) (Curtiss et al., 1995)) methodologies. Full geometry optimization of potentially stable structures was carried out at both levels of theory in DMSO and in chloroform solvents employing the polarizable continuum model (PCM) (Cossi et al., 2002). To ensure that this structure is a true energy minimum, its frequencies are calculated. There are not found any imaginary ones confirming that it is a true minimum structure. Thus, the global minima is obtained. All calculations have been performed and visualized using Gaussian 16 (Tzeli et al., 2016).

2.3. Induced fit docking

On the next stage, NGI25 was investigated for its potent binding to two major targets revealed from Swiss Target tool (http://www.swisstargetprediction.ch/) and bibliography (Ghafary et al., 2020; Peperidou et al., 2017) through molecular docking calculations. The crystal structures used for the *in silico* studies carried the following PDB IDs: *5T5V* (Offenbacher et al., 2017) and *4BDS* (Nachon et al., 2013). Protein preparation wizard, module available in Schrödinger Suites, was used to prepare the crystal structure for the *in silico* calculations. Since LOX is a metalloprotein, it has been considered that there are several computational challenges that need to be addressed, in comparison with BCHE. In order to take account of the quantum effects associated with the presence of a Fe^{3+} cation in LOX's active site, we used the 'create zero-order bonds to metals' module of the Schrödinger's Maestro molecular modeling platform. This module breaks existing bonds to metals -since they cannot be examined through the over-simplified model of a spring attached to a hard sphere- adds new zero-order bonds between metals and nearby atoms and corrects their formal charges accordingly, to constrain the X-ray acquired coordination geometry.

The cinnamic derivative was sketched in Schrodinger's Maestro (Schrodinger LLC, 2013a) molecular modeling platform and it was initially minimized using Macromodel (Schrodinger LLC, 2013b) and DFT calculations. LigPrep was used to prepare the 3D models, restricted to the specific stereochemistry of each molecule. During the ligand preparation the 'add metal binding states' option of the Epik module of LigPrep was chosen in order to create ligand binding states that are suitable for metal binding that would have been rejected otherwise, due to high energy state penalties. The geometries were optimized with MacroModel in order to relax the structures while chiral centers retained the proper chiralities. The force field used for minimization was OPLS2005 (Jorgensen et al., 1996). NGI25 was subjected to proper treatment of their protonation states at physiological pH (∼7.4). Hammett and Taft methods have been implemented in conjunction with an ionization tool to generate chemically sensible 3D models. The three-dimensional ligands' structure was further minimized, more rigorously, by MacroModel with water as solvent and OPLS2005 as force field, using a conjugate gradient (CG) method with a threshold of 0.01 kcal/mol. The minimized structure was further used as input to a mixed-torsional/low-sampling conformational search forced to keep the input chiralities. Conformational search generated a number of conformers for each molecule under study and the conformers were energetically ranked. The most favored conformation was used as input for the following docking calculations.

Docking calculations have been performed to reveal the possible binding of NGI25 to LOX-1 and BCHE. The calculations were performed with the Induced Fit Docking (IFD) method. The ligand was docked in the 10 energetically favored conformations generated by Macromodel. Protein preparation constrained refinement was applied in the Glide docking stage. Trimming side chains automatically (based on B – factor) and Prime refinement of the protein side chains were applied and the docking process was accomplished by Glide/XP. Finally, the binding energy for each target was calculated. The active site was described using a dielectric constant of 80 and all the crystallographic waters of the active site were preserved.

The same procedure was applied for two known inhibitors of these enzymes, that were retrieved from bibliography in order to serve as model-molecules for the evaluation of NGI's action towards the enzymes. The two inhibitors are zileuton (Carter et al., 1991) for LOX and rivastigmine for BCHE (Pohanka, 2014).
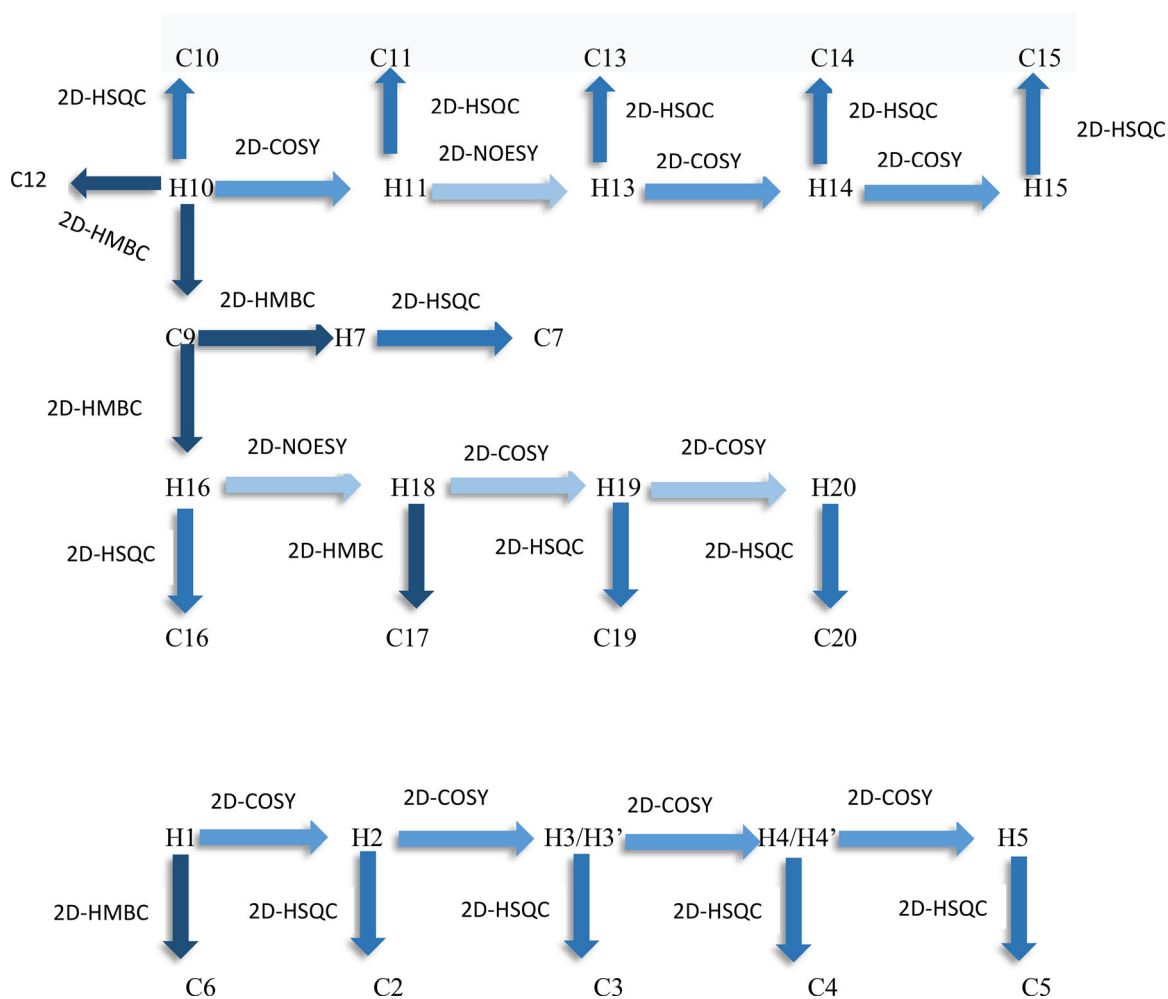
Figure 2. Overall diagram showing the identification strategy of the NGI25 compound in DMSO and CDCl3 solvents. Identification of the peaks are shown in Figures 3(a, b).

2.4. Molecular mechanics/generalized born surface area (MM/GBSA)

MM/GBSA was used to examine the stability of protein-ligand complexes through the calculation of free binding energy. MM/GBSA equations were extended to complex structures using the Prime module of Maestro. The three statistically predominant ligand-protein complexes that derived from MD trajectory cluster analysis were subjected to MM/GBSA calculations. VSGB solvation model which is realistic parametrization of the solvation and OPLS-2005 forcefield were used for protein flexibility (Pattar et al., 2020).

The binding energy is calculated according to the equation:

$$\Delta G \text{ bind} = E_{complex}(\text{minimized}) - E_{ligand}(\text{minimized}) - E_{receptor}(\text{minimized})$$

3. Results and discussion

3.1. Synthesis of NGI-25

The synthesis of the studied Ugi-4CR adduct NGI25 is summarized in Scheme 1. Using cinnamic acid, benzylamine, formaldehyde and cyclohexyl isocyanide in methanol at room temperature, this experimentally simple, atom-economical and versatile multicomponent reaction provided, after chromatographic purification, the Ugi adduct.

3.2. Strategy applied for the structure assignment of NGI25 in DMSO

As a convenient starting point for the structure assignment of NGI25 was used the readily assigned in the ^{1}H NMR spectrum, H-10. This resonates at 7.08 ppm as it is easily recognizable by its integration and doublet peak due to its coupling to H-11. H-11 can be easily identified to resonate at 7.54 ppm through 2D-COSY, as it is correlated through bond with H-10. H-11 is more deshielded than H-10 as expected due to its conjugation with the double bond. H-11 is correlated with two H-10s indicating that is involved in two conformations. Through 2D HSQC the H-10 and H-11 show [1]J$_{C-H}$ coupling with the C10 and C11, respectively, and therefore C10 and C11 are assigned unambiguously at 118.0 and 143.0 ppm, respectively.

Through 2D-NOESY, H-13 is identified at 7.67 ppm due to its spatial correlation with H-11. H-14 and H-15 are then identified through 2D-COSY due to their correlation with H-13 and H-14, respectively. Through 2D HSQC, the H-13, H-14 and H-15
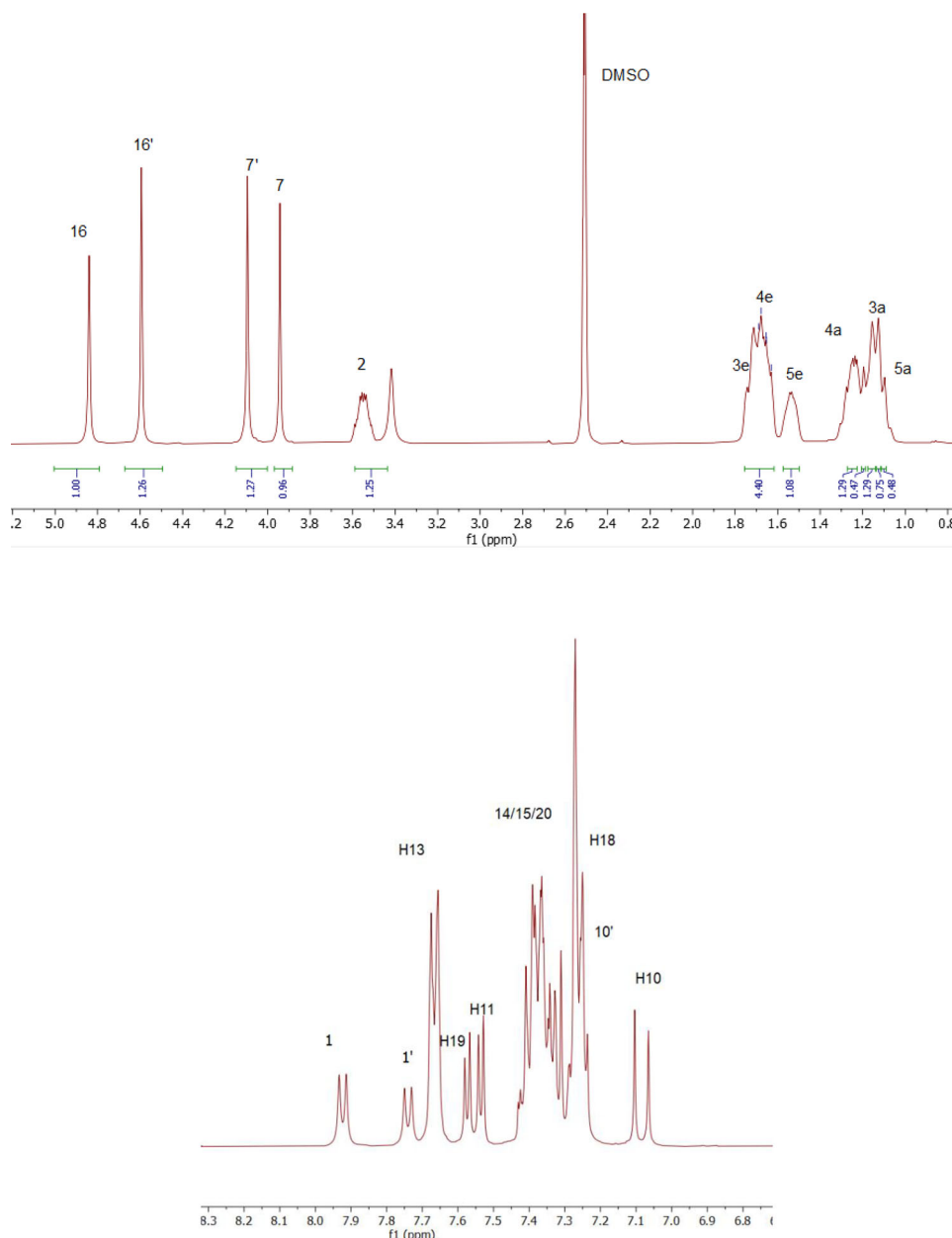
Figure 3A ^{1}H-NMR spectra: (top) Aliphatic region of NGI25 (bottom) aromatic region. The spectra were recorded in DMSO-d$_6$ on a Bruker AC 400 MHz spectrometer at ambient temperature.

show $^1J_{C-H}$ coupling with the C13, C14 and C15, respectively, and therefore C13, C14 and C15 are assigned unambiguously at 128.0, 128.0 and 130.0 ppm correspondingly.

The strategy proceeded in the region 4–5 ppm of the ^{1}H-spectra. Through 2D-NOESY, it is observed that peaks at 4.60 and 4.85 ppm correlate with proton at 7.25 ppm. It is easily understood that this latter peak is due to H-18, as it is correlated through space with H16. Through 2D-COSY, H-19 and H-20 are recognized due to their correlation with H-18 and H-19, respectively. Through 2D HSQC the H18, H-19 and H-20 show $^1J_{C-H}$ coupling with the C18, C19 and C20 correspondingly and therefore C18, C19 and C20 are assigned unambiguously at 127.6, 128.0 and 126.0 ppm, respectively.

The strategy proceeded by studying the aliphatic area. As it is mentioned earlier, H-16 is easily recognized to resonate at 4.60 and 4.85 ppm, due to its correlation with H-18. H-7 is

resonated at 3.95 and 4.10 ppm. Two peaks are observed which suggests that protons 16 and 7 can exist in two conformations. Through 2D HSQC the H-16 and H-7 show $^1J_{C-H}$ coupling with the C16 and C7, respectively, and therefore C16 and C7 are assigned unambiguously at 50.2/51.9 and 49.1/50.1 ppm, respectively, due to two conformations.

The peak at 3.54 ppm corresponds at H-2 due to its correlation with two doublet peaks at 7.75 and 7.91 ppm, respectively, through 2D-COSY. These doublet peaks correspond to two different conformations of NH-1, since H-2 cannot be associated with any other proton in the specific region of the spectrum. Through 2D-HSQC, H-2 shows $^1J_{C-H}$ coupling with the C2 resonated at 48.0 ppm.

The strategy was continued by obtaining more information from H-2 resonance. Cyclohexane has equatorial and axial protons. In the case where the group in the cyclohexane is in axial
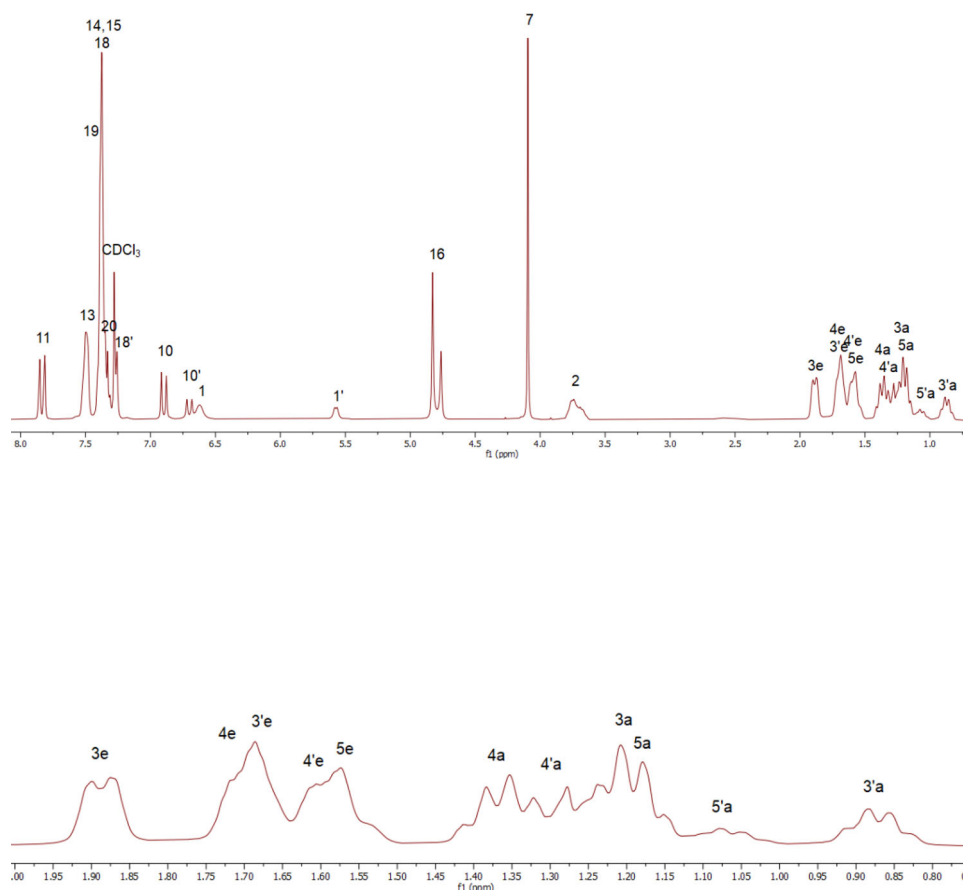
Figure 3B. ¹H-NMR spectra: (top) Full region (bottom) aliphatic region of NGI25. The spectra were recorded in CDCl₃ on a Bruker AC 400 MHz spectrometer at ambient temperature.

position there is a *gauche* interaction between this group and C4. This is absent in the conformation where the group is equatorial. This *gauche* interaction is an example of van der Waals strain, which is what makes the axial conformer higher in energy. The chemical shifts of equatorials and axial protons depend on the dihedral angle between protons and carbons. As a result, the equatorial protons are resonated to higher values of chemical shifts than axial protons (Booth, 1964; Nickon et al., 1963). H-3, H-4 and H-5 were recognized through 2D-COSY and 2D-NOESY. Specifically, the broad peak at 1.54 ppm with integration 1 is due to H-5eq. It is also observed that H-2 correlates with two protons at 1.75 and 1.14 ppm which will obviously correspond to H-3eq and H-3ax, respectively. H-4ax is recognized to resonate at 1.25 ppm due to its correlation with H-3eq. Moreover, H-4eq is recognized to resonate at 1.69 ppm due to its correlation with H-3ax. C3, C4 and C5 were identified through 2D-HSQC.

Through two-dimensional ¹³C-¹H spectrum of the NGI25, all the carbons were identified except for the quaternary and carbonyl carbons. However, these carbons can be identified through 2D-HMBC. Carbonyls are resonated at 160–200 ppm. Specifically, H-10 shows $^2J_{C-H}$ coupling with C9 and H-1 shows $^2J_{C-H}$ coupling with C6. It is observed that C6 is slightly more deshielded than C9 (Nummert et al., 2009). Continuing with the identification of quaternary carbons, in ¹³C spectrum two peaks are observed at 135.0 and 137.5 ppm, which have not been identified yet. These will be carbons 12 and 17, respectively. Through 2D-HMBC, H-10 shows $^3J_{C-H}$ coupling with C12 and H-18 shows $^2J_{C-H}$

coupling with C17. Based on this strategy, the complete identification of all the proton and carbon atoms of the NGI25 molecule was achieved (see the strategy Figure 2).

Figures 3(a, b) show ¹H and ¹³C chemical shift assignments of NGI25 in CDCl₃ and DMSO-d₆, respectively. The 1D and 2D spectra of NGI25 in the two environments are shown in Supporting Information.

3.3. Grid scan

The angles of NGI25 that were selected for the application of Grid Scan methodology are formed by the following atoms: **7-8(N)-9-10 (τ_1)** and by **6-7-8(N)-9 (τ_2).** The critical dihedral angles have been rotated in order to achieve the energy minima and maxima.

Through the rotation of τ_1 and τ_2 by 10°, we obtained the lowest conformations that are depicted when the dihedrals are 180.3° and 89.9°, respectively (Figure 4).

The minimized conformation obtained from the rotation of dihedral angle τ_1 was used as a starting structure for the next grid scan. A second grid scan search was performed from the rotation of dihedral angle τ_2 and a new minimized structure was derived.

3.4. Conformational analysis using molecular dynamics

The derived from grid scan minimized conformation of NGI25 was used as input to Molecular Dynamics studies.
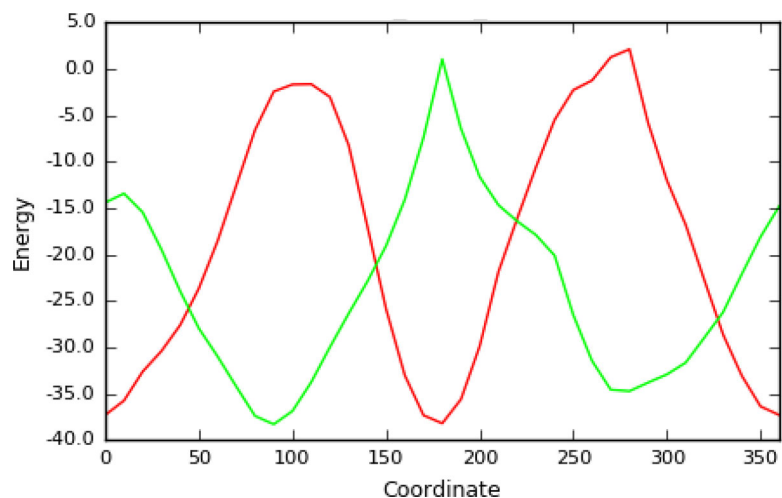
Figure 4. Energy (kj/mol) vs dihedral angle (coordinate). Rotation of τ_1, τ_2 angles by 10° produces an energy minimum at 180.3° (red) and 89.9° (green), respectively.
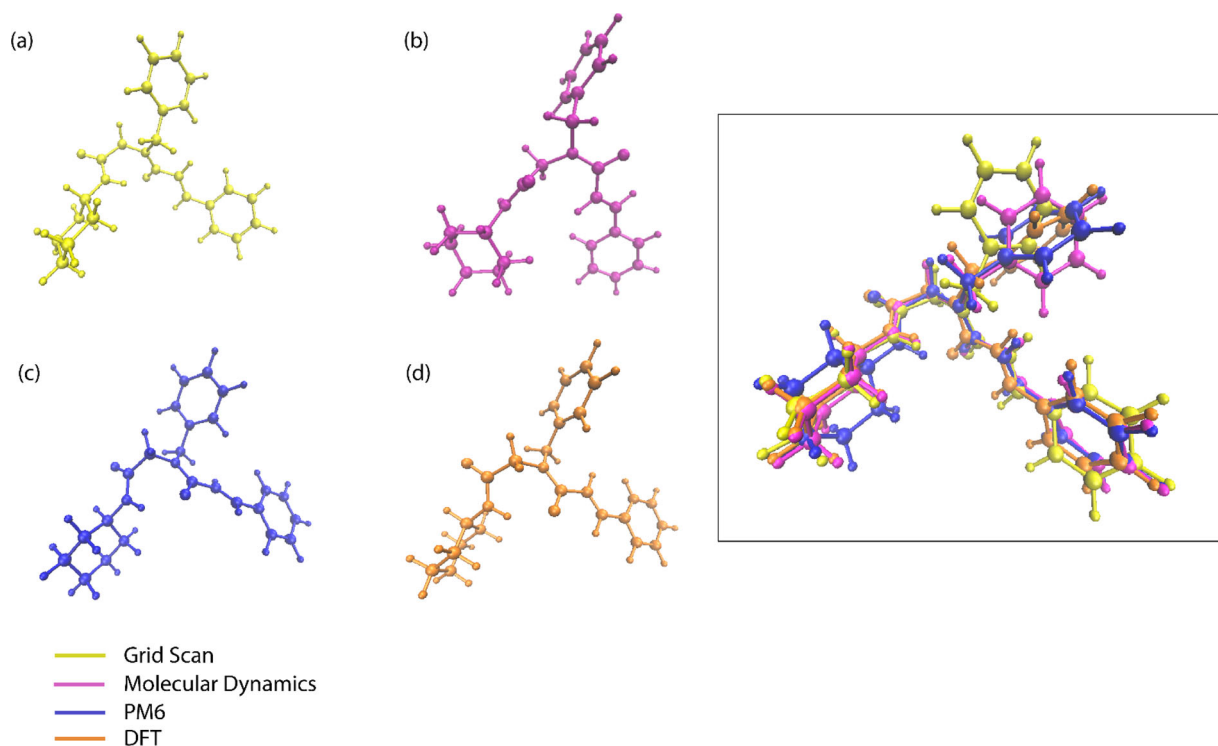

Figure 5. Conformation of NGI25 derived from (**a**) Grid scan (**b**) Molecular Dynamics (**c**) PM6 (**d**) DFT (B3LYP/6-311 + G(d,p)) methodologies. The superimposition of these conformers is illustrated in the framed part of the figure.

Trajectory cluster analysis was performed for the 500 ns of the simulations. The trajectory was divided in 10 clusters based on the cinnamic compound's conformations that were adopted during the simulations. Cluster analysis can be used to identify discrete conformations in this ensemble by identifying groups of conformers that have similar geometries according to a chosen metric. The most probable conformation that was adopted for 41% of the simulation time is illustrated in Figure 5(b) (NGI25 in DMSO), Identical results were also shown with chloroform solvent. MD studies suggest that the two aromatic rings of the compound are almost vertical between each other in both solvents tested. This result compliments the NMR experimental results, where no NOE correlations were observed between the protons of the two aromatic rings in 2D

NOESY spectrum. Furthermore, the long distance of the cyclohexane part of the compound from both aromatic rings is also in agreement with the NMR conformational studies, since no NOEs have been observed between cyclohexane's and aromatic protons (Imtiaz, Muzaffar, et al., 2021).

3.5. Conformational analysis with semi-empirical and QM methods

Figure 5 indicates all the conformations acquired by the application of different methods in order to discover the conformational properties of NGI25. NGI's conformations do not present important differences between the results of all the computational methods and experimental NMR results.
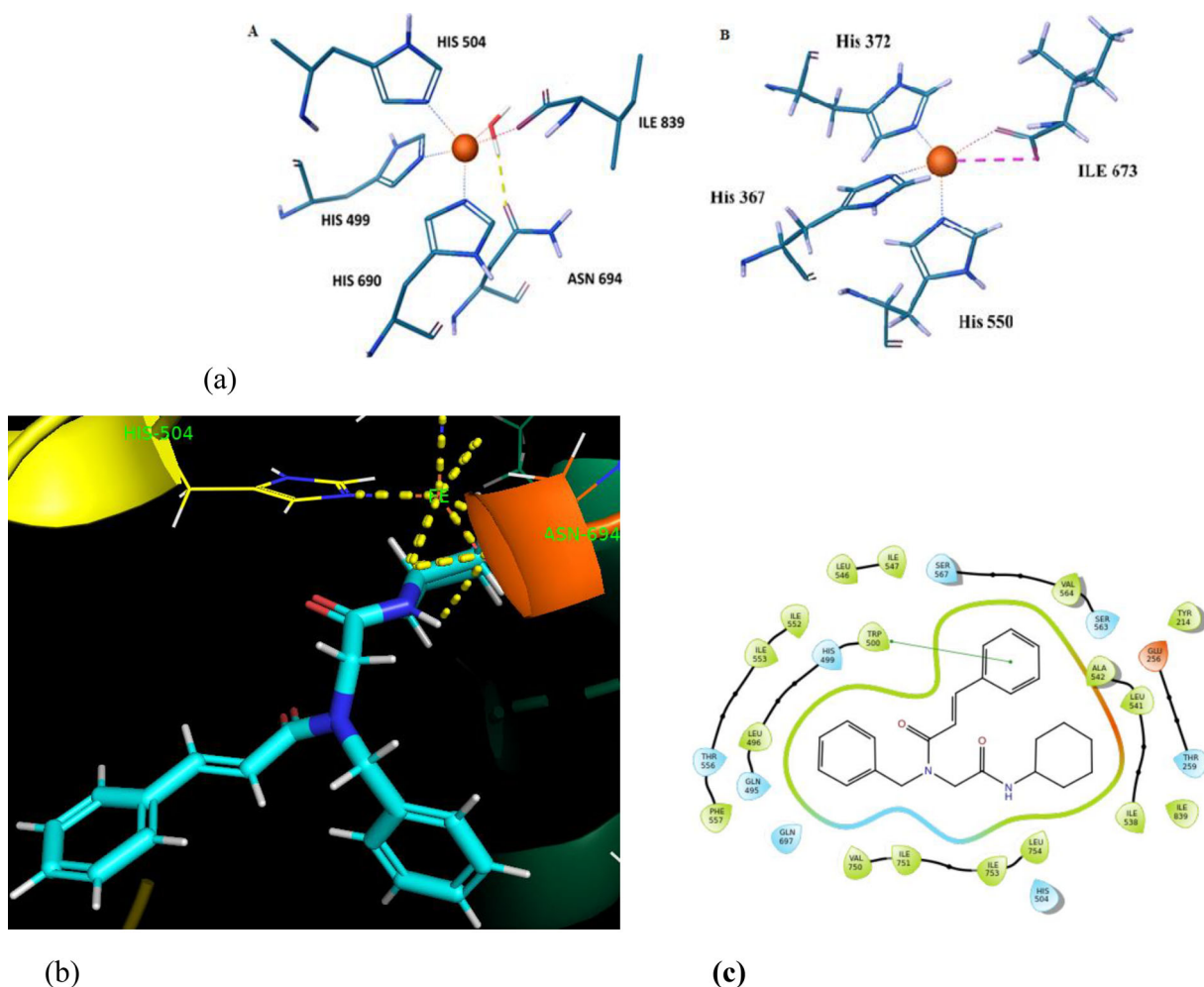
Figure 6. (a) Active site of LOX. Interactions between NGI25 with the residues of LOX in (b) 3D structure and (c) 2D structure.
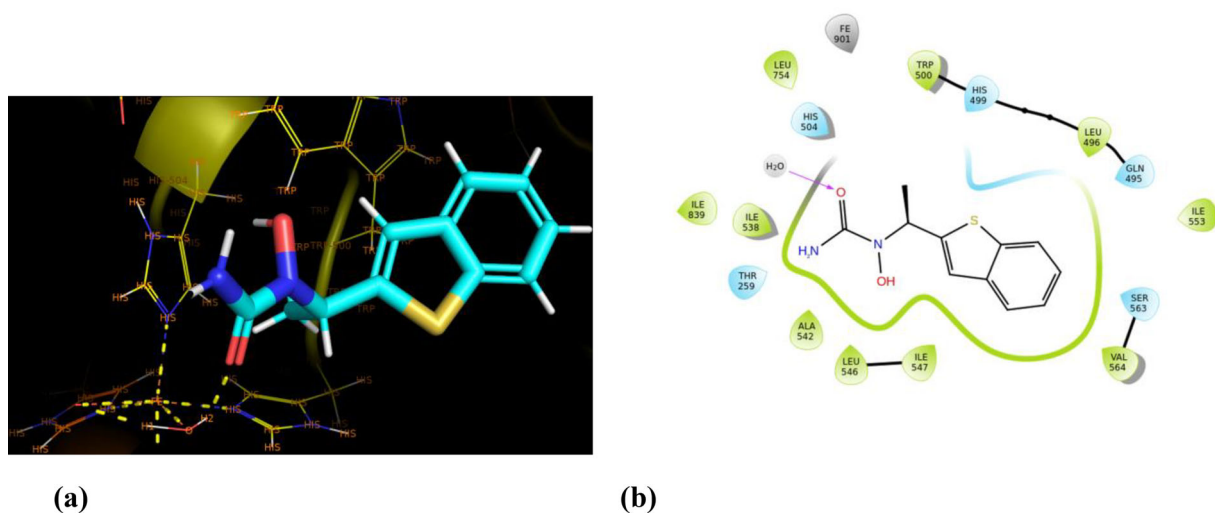

Figure 7. Interactions between zileuton with the residues of LOX in (a) 3D structure and (b) 2D structure.

In particular, the conformations provided by Grid Scan, MD, PM6 and DFT methodology are quite similar (see Figure 5), and only minor differences between the conformers that derived from PM6 and DFT calculations are observed. MD studies suggest a flip of 60° for one of the aromatic rings, while grid scan indicates that the same ring is a little displaced in comparison with the DFT and PM6 conformations. The superimposition of these conformers pinpoints that no important conformational differences are observed among them. All the conformations revealed by computational studies compliment the experimental results analyzed in paragraph 3.2. In fact, these conformations indicate that
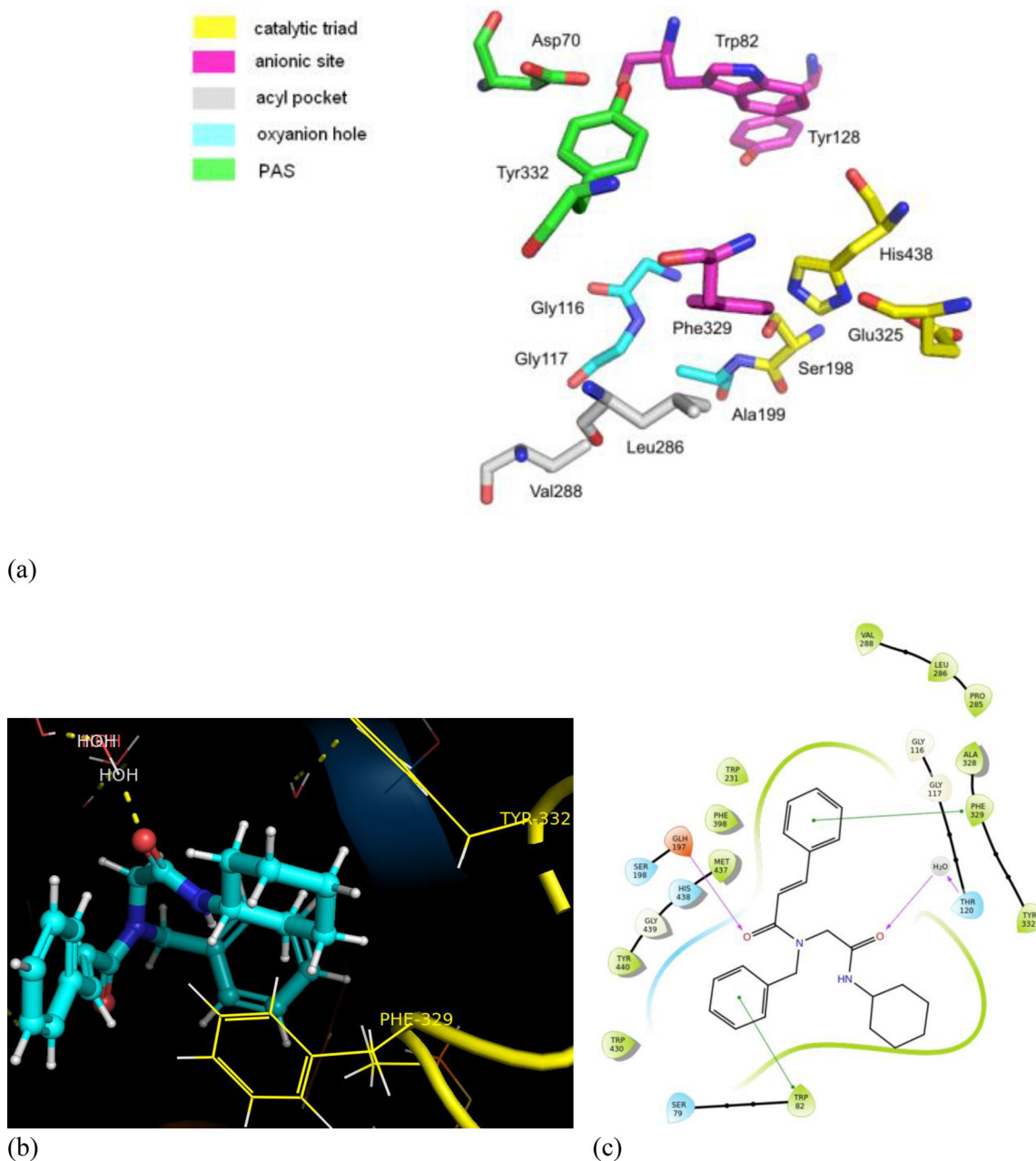
Figure 8. (a) Active site of BCHE. Interactions between NGI25 with the residues of BCHE in (b) 3D structure and (c) 2D structure.

the two aromatic rings are almost vertical between each other, justifying the absence of NOE correlations in the aromatic region in 2D NOESY spectra. The two conformations of NGI25 are due to N8-C9 tertiary amide bond. Finally, the vicinal proximity of the cyclohexyl part of the NGI with the aromatic ring is in accordance with the obtained 2D NOESY spectra, where NOEs are observed between these parts of the molecule.

3.6. Molecular binding

Induced Fit docking was applied in order to reveal the potent binding of NGI25 to the two aforementioned enzyme-targets (LOX-1 and BCHE) (Imtiaz, Banoo, et al., 2021; Kuca et al., 2018).

3.6.1. LOX

The active site of LOXs is characterized by a Fe cation coordinated by 3 histidine residues and 1 isoleucine residue. Given the fact that the active site of LOX isoforms follows a certain pattern, we can assume that a strong binder of soybean LOX could also possibly bind to the active site of human 5-LOX, as well as other LOX isoforms. Figure 6(a) below shows the high similarity of the active sites of two different LOX soybean LOX-1 (left) and 5-LOX (right) (Newcomer & Brash, 2015). NGI25 binds strongly to the active site of LOX-1 with docking score, $\Delta G_{bind} = -12.20$ kcal/mol. In particular, NGI25 forms one hydrogen bond, which is illustrated in yellow (Figure 7(b)), between NH and the water molecule coordinating the catalytic Fe. Moreover, a π-π stacking interaction is formed between the aromatic ring of NGI25 and TRP500, which is a critical residue in LOX's cavity. Furthermore, the
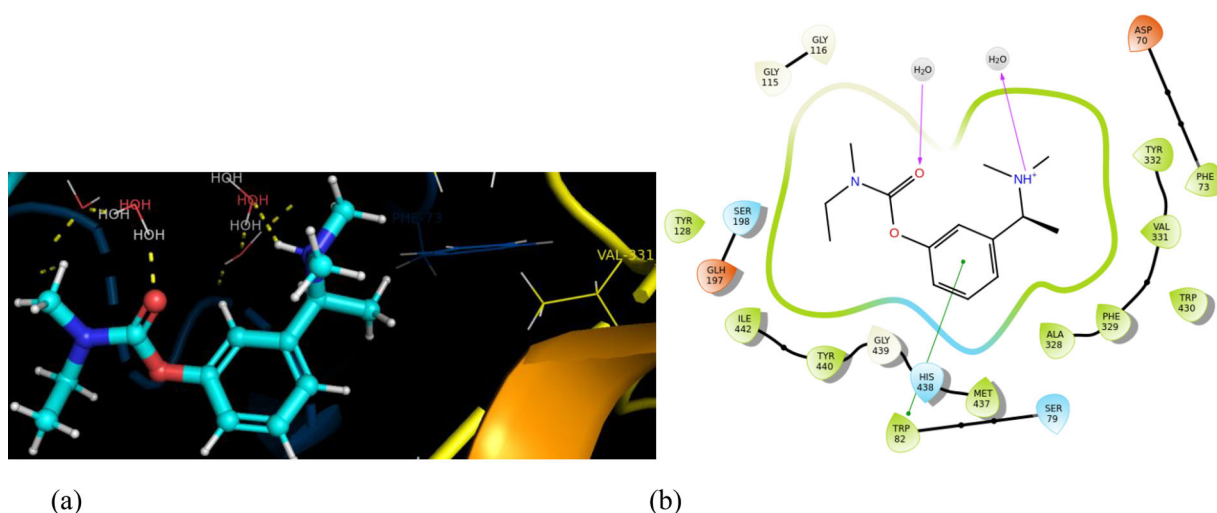
Figure 9. Interactions between rivastigmine with residues of BCHE in **(a)** 3D structure and **(b)** 2D structure.
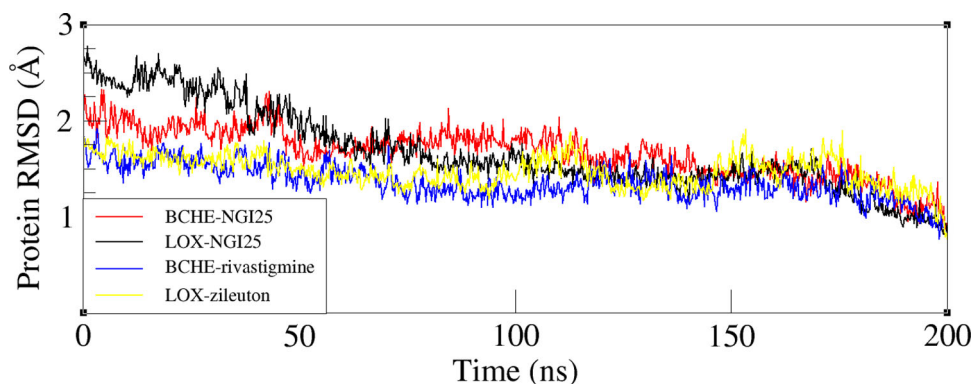

Figure 10. RMSD values of proteins in 'enzyme-ligand' complexes for 200 ns of the simulation taking as reference structure the pose derived by docking studies.
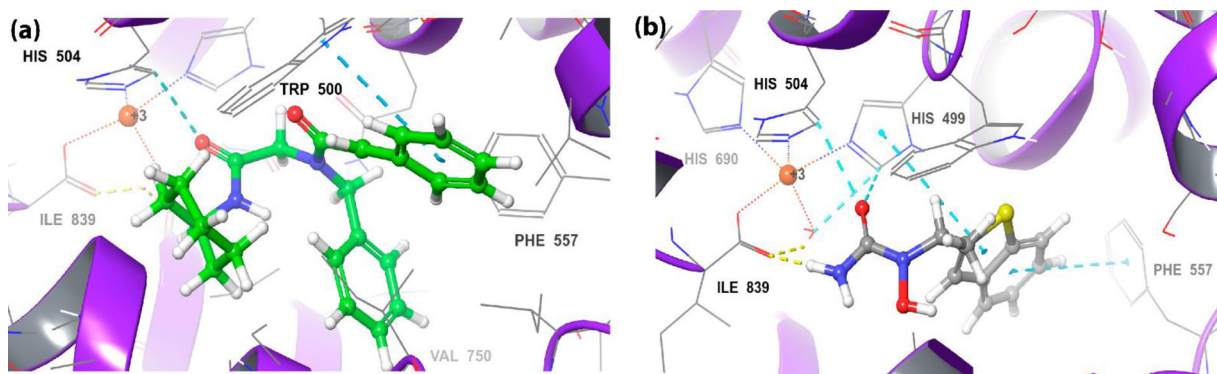

Figure 11. 3D poses of **(a)** NGI25 and **(b)** zileuton in LOX's cavity. Both poses were derived from the most predominant cluster of the correspondent MD simulations.

hydrophobic part of the molecule is oriented towards the lipophilic residues of the active site, i.e. TRP500, VALILE547, LEU546, LEU541, ALA542 (Figure 6(b)). In order to justify our *in silico* results, one known inhibitor has been selected for each enzyme-target so as to serve as a prototype in our docking studies. Zileuton which is known to inhibit LOX, according to our *in silico* results binds strongly to the active site of the enzyme with $\Delta G_{bind} = -8.56$ kcal/mol (Figure 7). This value is quite higher than the same value reported for NGI25, with an important difference of ~4kcal/mol. This

result pinpoints that the molecule under study could serve as a significant binder of LOX enzyme, since it forms more interactions with the enzyme's cavity.

3.6.2. BCHE
The active site of BCHE is coordinated by 13 amino acids. Especially, the catalytic triad contains three amino acids: SER198, GLU325 and HIS438 (Figure 8(a)) (Bajda et al., 2013). Furthermore, NGI25 binds strongly to BCHE indicating
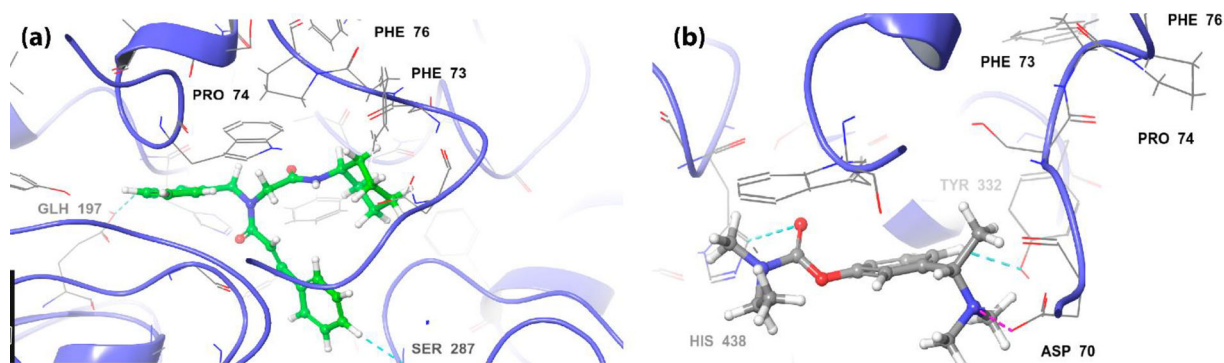
Figure 12. 3D poses of **(a)** NGI25 and **(b)** rivastigmine in BCHE's cavity. Both poses were derived from the most predominant cluster of the correspondent MD simulations.

Table 1. ΔG_{bind} of 'enzyme-ligand' complexes as calculated after MD studies.

Compounds in LOX	ΔG_{bind} MM/GBSA (kcal/mol)
Zileuton	−30.80
NGI25	−52.80
Compounds in BCHE	ΔG_{bind} MM/GBSA (kcal/mol)
Rivastigmine	−41.44
NGI25	−50.74

$\Delta G_{bind} = -11.59$ kcal/mol. In this case, NGI25 forms two hydrogen bonds with residue THR120 and a water molecule of the active site, while two π-π stacking interactions occur between the two aromatic rings of NGI25 and residues PHE329 and TRP82 (Figure 8(b)). Moreover, two aromatic hydrogen bonds are formed between two phenyl protons of NGI and the carbonyl group of HIS438. Finally, the aromatic rings and the cyclohexyl part of NGI are oriented towards the hydrophobic residues of the cavity, i.e. TRP231, ALA199, ALA328, PHE329, VAL331, TYR332.

The known inhibitor of BCHE that was selected in order to evaluate the docking results for NGI, was rivastigmine. Rivastigmine binds strongly to the active site of the BCHE with $\Delta G_{bind} = -10.05$ kcal/mol. The same value calculated for 'NGI-BCHE' complex was lower, indicating the NGI25 could be a significant anti-BCHE agent. Furthermore, some interactions that NGI forms with the residues of the active site are also observed during the formation of 'rivastigmine-BCHE' complex. These interactions include the π-π stacking between the aromatic ring of rivastigmine and TRP82, as well as the formation of a hydrogen bond with a water molecule residing into the active site. An additional interaction that is observed in 'rivastigmine-BCHE' complex is the formation of a pi-cation between the positively charged amine group of rivastigmine and the aromatic ring of TRP82. Finally, the hydrophobic part of rivastigmine is also oriented towards the same hydrophobic residues of the cavity, i.e. TRP231, ALA199, ALA328, PHE329, VAL331, TYR332 (Figure 9(a)).

3.7. Molecular dynamics of 'enzyme-ligand' complexes

Molecular Dynamics simulations have been performed to the four 'enzyme-ligand' complexes, that derived from molecular docking studies (Guimarães et al., 2011). The complex indicating the lowest ΔG_{bind} value for each ligand has been selected as starting structure for the MD studies. MD simulations illustrated that the ligands under study remained stable into the enzymes' cavities during the whole simulation time (200 ns). The RMSD diagram (Figure 10) indicates the stability of each system during the simulations.

During the simulation, ligands inside the enzymes' cavity, adopted slightly different, more favorable, conformations than the ones derived from docking studies. In order to further assess the ligands' stability, cluster analysis has been performed to the trajectories obtained for every complex. The trajectories have been divided into 10 clusters in order to reveal the conformation of the ligand that is statistically predominant during the simulation.

3.7.1. LOX

Trajectory cluster analysis in 'LOX-NGI25' complex revealed that the most predominant conformation of NGI inside the cavity lasts for 54% of the simulation time. The pose of NGI inside LOX's cavity is illustrated in Figure 11(a). NGI resides in vicinal proximity with the catalytic Fe in LOX's active site (∼2.9 Å), while it forms a π-π interaction with TRP500, which is a critical residue of the enzyme's cavity. This interaction has been previously observed by docking studies. Furthermore, an aromatic hydrogen bond is formed between the carbonyl group of NGI25 residing close to cyclohexane and the aromatic proton of HIS504, which is a residue in the first sphere of Fe cooordination. Moreover, the hydrophobic part of the molecule (aromatic rings) is oriented towards the hydrophobic residues of the cavity, i.e. ILE553, ILE552, TRP500, PHE557, VAL750.

Similar interactions have been also observed for the 'LOX-zileuton' complex. The known LOX inhibitor, based on the pose that derived from the predominant cluster after MD studies (40% simulation time), forms a π-π interaction with HIS504 and HIS499 with its carbonyl group. Moreover, the aromatic substructure of the molecule forms two πi-π cations with residues PHE557 and HIS499. Finally, one hydrogen bond is observed between the proton of NGI's amine group and ILE839 of the cavity Figure 11(b).

3.7.2. BCHE

Trajectory cluster analysis in 'BCHE-NGI25' complex revealed that the most predominant conformation of NGI inside the

active site lasts for 39% of the simulation time. The pose of NGI inside the cavity is illustrated in Figure 12(a). NGI forms an hydrogen bond between the phenyl proton of the aromatic ring and the carbonyl group of SER287. Furthermore, another aromatic H-bond is observed between the carboxyl group of GLU197 and the proton of the second aromatic ring of NGI. Moreover, the hydrophobic part of the molecule (aromatic rings and cyclohexane) is oriented towards the hydrophobic residues of the cavity, i.e. PHE76, PHE73, PRO74.

The known BCHE inhibitor, rivastigmine, based on the pose that derived from the predominant cluster after MD studies (21% simulation time), resides in the same cavity as the NGI, which is the active site. The lipophilic part of the molecule is also oriented towards the hydrophobic residues, PHE76, PHE74, PRO73, while a salt bridge is formed between the positively charged amine group of rivastigmine and the carboxyl of ASP70. Finally, two aromatic H-bonds are observed between the inhibitor and the residues HIS438 and TYR332 of the active site (Figure 12(b)).

3.8. MM/GBSA calculations

MM/GBSA calculations have been applied to the statistically predominant 'enzyme-ligand' complexes that derived from Desmond trajectory clustering. In the table below (Table 1), the binding energies of NGI25 and known inhibitors for both enzymes are illustrated. According to the ΔG_{bind} values that are presented in the table, NGI25 binds favourably to the active site of both enzymes and the ΔG value is lower for NGI25 compared to the corresponding value for the known inhibitors. In LOX's cavity, for the most prominent cluster of NGI25 (54% of the simulation time), ΔG_{bind} is calculated at −52.80 kcal/mol, while for zileuton (40% of the simulation time) ΔG_{bind} value is quite lower (−30.80 kcal/mol). Finally, in BCHE's active site, for the most prominent cluster of NGI25 (39% of the simulation time), ΔG_{bind} is calculated at −50.74 kcal/mol, while for rivastigmine (21% of the simulation time) ΔG_{bind} value is lower (−41.44 kcal/mol). The results are illustrated in Table 1.

4. Conclusions

This study focused on the conformational analysis of cinnamic derivative NGI25 as determined by a combination of NMR spectroscopy and computational studies (MM, MD and QM). The conformational analysis of NGI25 indicated that the molecule adopts similar conformations in DMSO and CHCl$_3$ solvents. The most important conformational property of the molecule is the orthogonality between the two aromatic rings which is supported by the experimental data and confirmed by the theoretical ones.

Through extended bibliography research and use of SwissTarget module, NGI25 was discovered as a possible binder of butyrylcholinesterase and lipoxygenase enzymes. Indeed, docking results that were performed confirmed this prediction. In particular, NGI25 indicated strong binding to both LOX's and BCHE's active site, with ΔG_{bind} calculated at −12.20 kcal/mol and −11.59 kcal/mol, respectively. One

known inhibitor has been selected for each enzyme in order to validate the observed binding energies. In both cases, NGI25 indicated lower binding energy to these enzymes than the prototypes, zileuton and rivastigmine, that were subjected to the same *in silico* studies. Furthermore, NGI25 remained stable inside both enzymes' active sites during the whole simulation time of the MD simulations. MM/GBSA calculations were performed in the most predominant cluster of the MD studies for all the 'enzyme-ligand' complexes. MM/GBSA results also confirmed the higher affinity of NGI25 to both enzymes' cavities compared to zileuton and rivastigmine.

NGI25 binds strongly in spatial proximity with catalytic Fe of LOX cavity and interacts with many of the critical residues of the active site, as it is also observed in several *in silico* studies for LOX inhibition (Chontzopoulou et al., 2021; Kuca et al., 2018). Moreover, the interactions that NGI forms with the critical residues of BCHE's active site are quite similar in a variety of BCHE's inhibitors that have been discovered in bibliography (Begum et al., 2018; Chontzopoulou et al., 2021; Katsori et al., 2011; Vrontaki et al., 2015). Hence, NGI25 could serve as an important agent to guide the drug design against Alzheimer and other neurological diseases. Taking everything into account, it will be illustrated soon if the drug design will lead successfully to new drugs. The information obtained regarding the conformational properties and the target prediction of NGI25 may also be of aid to synthetic chemists who wish to develop cinnamic analogs with better biological profiles and pharmacological properties.

ORCID

Thomas Mavromoustakos 🔴 http://orcid.org/0000-0001-5309-992X

References

Akritopoulou-Zanze, I. (2008). Isocyanide-based multicomponent reactions in drug discovery. *Current Opinion in Chemical Biology*, *12*(3), 324–331. https://doi.org/10.1016/j.cbpa.2008.02.004

Bajda, M., Więckowska, A., Hebda, M., Guzior, N., Sotriffer, C., & Malawska, B. (2013). Structure-based search for new inhibitors of cholinesterases. *International Journal of Molecular Sciences*, *14*(3), 5608–5632. https://doi.org/10.3390/ijms14035608

Basso, A., Banfi, L., & Riva, R. (2010). A marriage of convenience: Combining the power of isocyanide based multicomponent reactions with the versatility of (hetero)norbornene chemistry. *European Journal*

of Organic Chemistry, 2010(10), 1831–1841. https://doi.org/10.1002/ejoc.200901438

Becke, A. D. (1993). A new mixing of Hartree–Fock and local density-functional theories. Journal of Chemical Physics, 98(2), 1372–1377. https://doi.org/10.1063/1.464304

Begum, S., Nizami, S. S., Mahmood, U., Masood, S., Iftikhar, S., & Saied, S. (2018). In-vitro evaluation and in-silico studies applied on newly synthesized amide derivatives of N-phthaloylglycine as butyrylcholinesterase (BChE) inhibitors. Computational Biology and Chemistry, 74, 212–217. https://doi.org/10.1016/j.compbiolchem.2018.04.003

Booth, H. (1964). The average coupling constants of protons on adjacent carbon atoms in mobile cyclohexane systems. Tetrahedron, 20(10), 2211–2216. https://doi.org/10.1016/S0040-4020(01)97606-9

Carter, G. W., Young, P. R., Albert, D. H., Bouska, J., Dyer, R., Bell, R. L., Summers, J. B., & Brooks, D. W. (1991). 5-Lipoxygenase inhibitory activity of zileuton. The Journal of Pharmacology and Experimental Therapeutics, 256(3), 929–937.

Chontzopoulou, E., Papaemmanouil, C. D., Chatziathanasiadou, M. V., Kolokouris, D., Kiriakidi, S., Konstantinidi, A., Gerogianni, I., Tselios, T., Kostakis, I. K., Chrysina, E. D., Hadjipavlou-Litina, D., Tzeli, D., Tzakos, A. G., & Mavromoustakos, T. (2021). Molecular investigation of artificial and natural sweeteners as potential anti-inflammatory agents. Journal of Biomolecular Structure and Dynamics, 1–13. https://doi.org/10.1080/07391102.2021.1973565

Cioc, R. C., Ruijter, E., & Orru, R. V. A. (2014). Multicomponent reactions: Advanced tools for sustainable organic synthesis. Green Chemistry, 16(6), 2958–2975. https://doi.org/10.1039/C4GC00013G

Cossi, M., Scalmani, G., Rega, N., & Barone, V. (2002). New developments in the polarizable continuum model for quantum mechanical and classical calculations on molecules in solution. Journal of Chemical Physics, 117(1), 43–54. https://doi.org/10.1063/1.1480445

Curtiss, L. A., McGrath, M. P., Blaudeau, J., Davis, N. E., Binning, R. C., & Radom, L. (1995). Extension of Gaussian-2 theory to molecules containing third-row atoms Ga–Kr. Journal of Chemical Physics, 103(14), 6104–6113. https://doi.org/10.1063/1.470438

D. E. Shaw Research. Desmond tutorial. Schroedinger. https://www.deshawresearch.com/downloads/download_desmond_cgi/Desmond_Tutorial-0.6.pdf

Daina, A., Michielin, O., & Zoete, V. (2017). SwissADME: A free web tool to evaluate pharmacokinetics, drug-likeness and medicinal chemistry friendliness of small molecules. Scientific Reports, 7, 42717. https://doi.org/10.1038/srep42717

Dömling, A. (2006). Recent developments in isocyanide based multicomponent reactions in applied chemistry. Chemical Reviews, 106(1), 17–89. https://doi.org/10.1021/cr0505728

Dömling, A., Wang, W., & Wang, K. (2012). Chemistry and biology of multicomponent reactions. Chemical Reviews, 112(6), 3083–3135. https://doi.org/10.1021/cr100233r

Essmann, U., Perera, L., Berkowitz, M. L., Darden, T., Lee, H., & Pedersen, L. G. (1995). A smooth particle mesh Ewald method. Journal of Chemical Physics, 103(19), 8577–8593. https://doi.org/doi:10.1063/1.470117 https://doi.org/10.1063/1.470117

Fouad, M. A., Abdel-Hamid, H., & Ayoup, M. S. (2020). Two decades of recent advances of Ugi reactions: Synthetic and pharmaceutical applications. RSC Advances, 10(70), 42644–42681. https://doi.org/10.1039/D0RA07501A

Ghafary, S., Ghobadian, R., Mahdavi, M., Nadri, H., Moradi, A., Akbarzadeh, T., Najafi, Z., Sharifzadeh, M., Edraki, N., Moghadam, F. H., & Amini, M. (2020). Design, synthesis, and evaluation of novel cinnamic acid-tryptamine hybrid for inhibition of acetylcholinesterase and butyrylcholinesterase. Daru: Journal of Faculty of Pharmacy, Tehran University of Medical Sciences, 28(2), 463–477. https://doi.org/10.1007/s40199-020-00346-9

Graebin, C. S., Ribeiro, F. V., Rogério, K. R., & Kümmerle, A. E. (2019). Multicomponent reactions for the synthesis of bioactive compounds: A review. Current Organic Synthesis, 16(6), 855–899. https://doi.org/10.2174/1570179416666190718153703

Gruppen, B., Zerfall, T., Kennzeichnung, Z., Siedepunktsgleichung, E., Verbindung, E., Chloroform-Losungen, D., Absorptionsmaxima, D., & Ekment, E. (1959). Versammlungsberichte. Angewandte Chemie, 71(11), 373–388. https://doi.org/10.1002/ange.19590711110

Guimarães, A. P., Oliveira, A. A., da Cunha, E. F. F., Ramalho, T. C., & França, T. C. C. (2011). Design of new chemotherapeutics against the deadly anthrax disease. Docking and molecular dynamics studies of inhibitors containing pyrrolidine and riboamidrazone rings on nucleoside hydrolase from Bacillus anthracis. Journal of Biomolecular Structure & Dynamics, 28(4), 455–469. https://doi.org/10.1080/07391102.2011.10508588

Hulme, C., & Gore, V. (2003). "Multi-component reactions: Emerging chemistry in drug discovery" 'from xylocain to crixivan'. Current Medicinal Chemistry, 10(1), 51–80. https://doi.org/10.2174/0929867033368600

Humphreys, D. D., Friesner, R. A., & Berne, B. J. (1994). A multiple-time-step molecular dynamics algorithm for macromolecules. The Journal of Physical Chemistry, 98(27), 6885–6892. https://doi.org/doi:10.1021/j100078a035 https://doi.org/10.1021/j100078a035

Imtiaz, S., Banoo, S., Muzaffar, S., & Ali, S. M. (2021). Structural determination of midazolam/beta-cyclodextrin inclusion complex by an already proposed protocol and molecular docking studies by quantitative analysis. Structural Chemistry, 32(4), 1505–1516. https://doi.org/10.1007/s11224-021-01727-9

Imtiaz, S., Muzaffar, S., & Ali, S. M. (2021). Demonstrating accuracy of the already proposed protocol for structure elucidation of cyclodextrin inclusion complexes by validation using quantitative ROESY analysis. Journal of Inclusion Phenomena and Macrocyclic Chemistry, 100(1–2), 71–87. https://doi.org/10.1007/s10847-021-01047-9

Jieping Zhu, H. B. (2005). Multicomponent reactions. Wiley.

Jorgensen, W. L., Maxwell, D. S., & Tirado-Rives, J. (1996). Development and testing of the OPLS all-atom force field on conformational energetics and properties of organic liquids. Journal of the American Chemical Society, 118(45), 11225–11236. https://doi.org/10.1021/ja9621760

Katsori, A. M., Chatzopoulou, M., Dimas, K., Kontogiorgis, C., Patsilinakos, A., Trangas, T., & Hadjipavlou-Litina, D. (2011). Curcumin analogues as possible anti-proliferative & anti-inflammatory agents. European Journal of Medicinal Chemistry, 46(7), 2722–2735. https://doi.org/10.1016/j.ejmech.2011.03.060

Kuca, K., Musilek, K., Jun, D., Zdarova-Karasova, J., Nepovimova, E., Soukup, O., Hrabinova, M., Mikler, J., Franca, T. C. C., Da Cunha, E. F. F., De Castro, A. A., Valis, M., & Ramalho, T. C. (2018). A newly developed oxime K203 is the most effective reactivator of tabun-inhibited acetylcholinesterase. BMC Pharmacology and Toxicology, 19(1), 8. https://doi.org/10.1186/s40360-018-0196-3

Lee, C., Yang, W., & Parr, R. G. (1988). Development of the Colle-Salvetti correlation-energy formula into a functional of the electron density. Physical Review. B, Condensed Matter, 37(2), 785–789. https://doi.org/10.1103/physrevb.37.785

Luo, J., Chen, G. S., Chen, S. J., Li, Z. D., & Liu, Y. L. (2021). Catalytic enantioselective isocyanide-based reactions: Beyond Passerini and Ugi multicomponent reactions. Chemistry (Weinheim an Der Bergstrasse, Germany), 27(22), 6598–6619. https://doi.org/10.1002/chem.202003224

Lyman, E., & Zuckerman, D. M. (2006). Ensemble-based convergence analysis of biomolecular trajectories. Biophysical Journal, 91(1), 164–172. https://doi.org/doi:10.1529/biophysj.106.082941

Martyna, G. J., Tobias, D. J., & Klein, M. L. (1994). Constant pressure molecular dynamics algorithms. Journal of Chemical Physics, 101(5), 4177–4189. https://doi.org/doi:10.1063/1.467468 https://doi.org/10.1063/1.467468

Nachon, F., Carletti, E., Ronco, C., Trovaslet, M., Nicolet, Y., Jean, L., & Renard, P.-Y. (2013). Crystal structures of human cholinesterases in complex with huprine W and tacrine: Elements of specificity for anti-Alzheimer's drugs targeting acetyl- and butyryl-cholinesterase. The Biochemical Journal, 453(3), 393–399. https://doi.org/10.1042/BJ20130013

Newcomer, M. E., & Brash, A. R. (2015). The structural basis for specificity in lipoxygenase catalysis. Protein Science: A Publication of the Protein Society, 24(3), 298–309. https://doi.org/10.1002/pro.2626

Nickon, A., Castle, M. A., Harada, R., Berkoff, C. E., & Williams, R. O. (1963). Chemical shifts of axial and equatorial α-protons in the N.M.R. of steroidal α-haloketones. Journal of the American Chemical Society, 85(14), 2185–2186. https://doi.org/10.1021/ja00897a047

Nummert, V., Piirsalu, M., Mäemets, V., Vahur, S., & Koppel, I. A. (2009). Effect of ortho substituents on carbonyl carbon 13 C NMR chemical shifts in substituted phenyl benzoates. *Journal of Physical Organic Chemistry*, 22(12), 1155–1165. https://doi.org/10.1002/poc.1569

Offenbacher, A. R., Hu, S., Poss, E. M., Carr, C. A. M., Scouras, A. D., Prigozhin, D. M., Iavarone, A. T., Palla, A., Alber, T., Fraser, J. S., & Klinman, J. P. (2017). Hydrogen-deuterium exchange of lipoxygenase uncovers a relationship between distal, solvent exposed protein motions and the thermal activation barrier for catalytic proton-coupled electron tunneling. *ACS Central Science*, 3(6), 570–579. https://doi.org/10.1021/acscentsci.7b00142

Pattar, S. V., Adhoni, S. A., Kamanavalli, C. M., & Kumbar, S. S. (2020). *In silico* molecular docking studies and MM/GBSA analysis of coumarin-carbonodithioate hybrid derivatives divulge the anticancer potential against breast cancer. *Beni-Suef University Journal of Basic and Applied Sciences*, 9(1), 36. https://doi.org/10.1186/s43088-020-00059-7

Peperidou, A., Pontiki, E., Hadjipavlou-Litina, D., Voulgari, E., & Avgoustakis, K. (2017). Multifunctional cinnamic acid derivatives. *Molecules*, 22(8), 1247. https://doi.org/10.3390/molecules22081247

Pohanka, M. (2014). Inhibitors of acetylcholinesterase and butyryl-cholinesterase meet immunity. *International Journal of Molecular Sciences*, 15(6), 9809–9825. https://doi.org/10.3390/ijms15069809

Ruijter, E., & Orru, R. V. A. (2013). Multicomponent reactions - Opportunities for the pharmaceutical industry . *Drug Discovery Today. Technologies*, 10(1), e15–e20. https://doi.org/10.1016/j.ddtec.2012.10.012

Schrodinger LLC. (2013a). *MacroModel*, Version 10.

Schrodinger LLC. (2013b). *MacroModel*, Version 10.2.

Theato, P. (2015). *Multi-component and sequential reactions in polymer synthesis - Advances in polymer science*. Springer International Publishing.

Touré, B. B., & Hall, D. G. (2009). Natural product synthesis using multi-component reaction strategies. *Chemical Reviews*, 109(9), 4439–4486. https://doi.org/10.1021/cr800296p

Tzeli, D., Kozielewicz, P., Zervou, M., Potamitis, C., Kokkotou, K., Rak, B., Petrou, A., Tsolaki, E., Gavalas, A., Geronikaki, A., Petsalakis, I. D., & Tsoungas, P. G. (2016). 2, 2′-Dihydroxybenzophenones and derivatives. Efficient synthesis and structure endoscopy by DFT and NMR. Credentials as potent anti-inflammatory agents. *ChemistrySelect*, 1(10), 2426–2438. https://doi.org/10.1002/slct.201600396

Vrontaki, E., Leonis, G., Avramopoulos, A., Papadopoulos, M. G., Simčič, M., Grdadolnik, S. G., Afantitis, A., Melagraki, G., Hadjikakou, S. K., & Mavromoustakos, T. (2015). Stability and binding effects of silver(I) complexes at lipoxygenase-1. *Journal of Enzyme Inhibition and Medicinal Chemistry*, 30(4), 539–549. https://doi.org/10.3109/14756366.2014.951348